Supplement of Atmos. Chem. Phys., 15, 7497–7522, 2015
http://www.atmos-chem-phys.net/15/7497/2015/
doi:10.5194/acp-15-7497-2015-supplement

Atmospheric Chemistry and Physics Open Access

Supplement of

Secondary organic aerosol formation from the β-pinene+NO_3 system: effect of humidity and peroxy radical fate

C. M. Boyd et al.

Correspondence to: N. L. Ng (ng@chbe.gatech.edu)

Formaldehyde needed for dry "RO_2+HO_2 dominant" Experiments

Formaldehyde is added to the chamber in order to enhance the RO_2+HO_2 chemistry. Without formaldehyde injection, simulation results based on the Master Chemical Mechanism (Equations are given at the end of Supplement) show that RO_2+RO_2 would be the dominant fate. However, once sufficient formaldehyde is added to the chamber experiments, we determine that the RO_2+HO_2 pathway is substantially greater than the RO_2+RO_2 pathway.

To determine the concentration of formaldehyde needed to favor the RO_2+HO_2 channel significantly over the RO_2+RO_2 channel, a comparison of relative reaction rates is required. Specifically, in order to favor a branching ratio of RO_2+HO_2 to RO_2+RO_2 by 95% (19:1), it is necessary that

$$k_{RO_2+HO_2}[HO_2][RO_2] = 19k_{RO_2+RO_2}[RO_2][RO_2] \quad \text{(SR1)}$$

$$k_{RO_2+HO_2}[HO_2] = 19k_{RO_2+RO_2}[RO_2] \quad \text{(SR2)}$$

$$k_{RO_2+HO_2}\frac{d[HO_2]}{dt} = 19k_{RO_2+RO_2}\frac{d[RO_2]}{dt} \quad \text{(SR3)}$$

Rates of production for each radical can then be used as a surrogate for the approximate concentrations as the radicals are expected to be consumed immediately upon production. The rates of production are:

$$\frac{d[HO_2]}{dt} = k_{HCHO+NO_3}[HCHO][NO_3] \quad \text{(SR4)}$$

$$\frac{d[RO_2]}{dt} = k_{\beta pin+NO_3}[\beta pin][NO_3] \quad \text{(SR5)}$$

Thus equation SR3 becomes:

$$k_{RO_2+HO_2}k_{HCHO+NO_3}[HCHO][NO_3] = 19k_{RO_2+RO_2}k_{\beta pin+NO_3}[\beta pin][NO_3] \quad \text{(SR6)}$$

$$k_{RO_2+HO_2}k_{HCHO+NO_3}[HCHO] = 19k_{RO_2+RO_2}k_{\beta pin+NO_3}[\beta pin] \quad \text{(SR7)}$$

Therefore, the ratio of formaldehyde to β-pinene should be ($k_{RO2+RO2}$ = 9.2E-14 cm^3 $molecules^{-1}$ s^{-1}; $k_{\beta pin+NO3}$ = 2.5E-12 cm^3 $molecules^{-1}$ s^{-1}; $k_{RO2+HO2}$ = 9.2E-14 cm^3 $molecules^{-1}$ s^{-1}; $k_{HCHO+NO3}$ = 5.5E-16 cm^3 $molecules^{-1}$ s^{-1}, all rate constants are from MCM v3.2 (Saunders et al., 2003)):

$$\frac{[HCHO]}{[\beta pin]} = \frac{19 k_{RO_2+RO_2} k_{\beta pin+NO_3}}{k_{RO_2+HO_2} k_{HCHO+NO_3}} = 350 \quad \text{(SR8)}$$

Results from Filter Sample Analysis

The UHPLC-MS total ion chromatogram for a typical "RO_2+NO_3 dominant" experiment under dry conditions is displayed in Fig. S5, which also represents the features observed in all other experiments under dry and humid conditions. Excluding the solvent peak at ~0.2 min and discarding the presence of any relevant species in the controls, the chromatogram in Fig. S5 reveals peaks with retention times of 3.26, 3.28, 6.19, 6.27, 7.03, and 7.08 min. These peaks are displayed in the extracted ion chromatograms (EIC) for species with *m/z* 489, 244, 473, 489, 505 and 522.

The collisional induced dissociation (CID) of the peak at ~3.26 min is displayed in Fig. S6 for the interval 30-70 V. Clearly, two anions with *m/z* 244 and 489 are observed at 3.26 min under low fragmentation voltage (30 and 40 V). The prominent peak *m/z* 290 is mainly due the presence of an adduct of the parent peak with formic acid: [M-H] + HCOOH = 244 + 46 = 290. Support for the previous observation is also based on the appearance of the adduct [M-H] + CH_3COOH = 244 + 60 = 304 in the presence of acetic acid, instead of formic acid, in the mobile phase. The ion observed at *m/z* 197 becomes more intense at higher fragmentation voltage before starting to break apart above 60 V. The parent peak *m/z* 244 must undergo the concerted loss of nitrous acid, HNO_2, to produce *m/z* 197. The loss of HNO_2 explains the change from an even to an odd mass, which may be facilitated by intramolecular hydrogen transfer from the hydroxyl group to the leaving -NO_2 moiety, leaving a carboxylate group as a rearranged fragment. The confirmation of the presence of a –COOH group in the neutral molecule with molecular mass 245 amu arises from the decarboxylative loss of 44 amu from the fragment ion *m/z* 197 that generates a new fragment at *m/z* 153.

The MS peak at *m/z* 489 in Fig. S6 does not show the formation of either a formic acid or an acetic acid adduct. In addition, the lack of a constant ratio for the ion count of species at *m/z* 244 and 489 in all experiments suggests that different formation pathways result in both products. The careful analysis of the data presented showing the formation of formate or acetate adducts for the species at *m/z* 244, and its excellent ionization at very low fragmentation voltage suggest that the co-eluting species at *m/z* 489 should be a carboxylic acid molecule in the mechanistic scheme (Fig. S7) to be presented below.

The chromatographic peak eluting at 6.19 min in Fig. S5 displayed as an EIC for *m/z* 505 with broad features corresponds to a species with molecular weight (MW) of 506 amu. Given the nitrogen rule, this species with even MW must contain an even number of nitrogen atoms. The combination of two β-pinene molecules, which have incorporated nitrate radicals, provides a starting mass of 396 amu for this species. The mass difference (506 – 396) amu = 110 amu eliminates the possibility of including a third β-pinene molecule or two more nitrate radicals in this product. Therefore, a general formula of $C_{20}H_{30}N_2O_{13}$ is assigned to this species. The ring and double bond equivalency (RDB) defines the number of unsaturated bonds in the compound:

$$RDB = 1 + \frac{\sum_i^{imax} N_i(V_i - 2)}{2} \qquad \text{(SR17)}$$

where i_{max} is the total number of different elements in the molecular formula, N_i is the number of atoms of element i, and V_i is the valence of atom I (Pavia et al., 2008). For $C_{20}H_{30}N_2O_{13}$, RDB = 7 from limiting the calculated formulas that make sense chemically, a -C=O group should be included in the structures of the mechanism forming species with this MW. Similarly, the EIC for *m/*z 522 shows a broad peak that could correspond to a less polar isomer species eluting at 6.27 min. A molecular structure with two β-pinene units and an odd number of nitrogen atoms is assigned to be $C_{20}H_{33}N_3O_{13}$ (MW = 523 amu) with RDB = 6 in the mechanism presented below.

Remarkably, a second species with *m/z* 489 elutes at 7.09 min in the EIC of Fig. S5, which possesses a carbonyl group absorbing with λ_{max} = 275 nm in the UV-visible spectrum. This molecule elutes later in the chromatogram, in the region of species with lower polarity –without a -COOH group– because it corresponds to a less polar structural isomer than that eluting at 3.26

min. The most likely general formula for this species is $C_{20}H_{30}N_2O_{12}$ (MW = 490) with RDB = 7, shown as the non-carboxylic acid structure in the mechanism introduced in the next section. A slightly lighter species with *m/z* 473 (MW = 474 amu) and retention time of 7.03 min also contains a carbonyl group in the UV-visible spectrum. The even molecular weight of this molecule indicates a species with an even number of nitrogen atoms. The similar retention times between both species (*m/z* 474 and 490) and the mass difference of only 16 amu suggests a common molecular structure that differs by one oxygen atom. The molecular formula $C_{20}H_{33}N_2O_{11}$ (MW = 474 amu) is represented by the proposed structures displayed in Fig. S7.

Figure S7 shows the further oxidation of some of the products shown in Fig. 8 of the main text. Panel A of Fig. S7 shows the hydroxycarbonyl nitrate product with MW = 229 amu can be further oxidized to the peroxy radical **V** by hydrogen abstraction from C_4 (R27) and subsequent reaction with oxygen (R28). Hydrogen abstraction from the dihydroxycarbonyl nitrate generated from **V** by R29 occurs preferentially on a $-CH_3$ group (C_9 or C_{10}) by R30, proceeding through an alkyl radical with true trigonal pyramidal geometry, an unfavorable intermediate for C_5, C_7, and C_8 due to the geometric constrains imposed by the cyclobutane ring (Vereecken and Peeters, 2012). Less likely is the abstraction occurring at C_4, due to both the hindrance created by the alcohol substituent and the slight strain from the adjacent butane ring. Addition of O_2 is also included in R30 (Atkinson and Arey, 2003), resulting in a peroxy radical **W**. Reaction R31 for **W** + **L**$^{\bullet}$ produces an alcohol ($R^{31}OH$) which can undergo a second H-abstraction by step 1 of R32 at the same carbon, C_{10}. C_{10} is slightly more electropositive than C_9 due to the hydroxyl substituent, and abstraction of the only H remaining at the more hindered C_4 of W is less likely to occur than at C_{10}. Step 2 of R32 shows the formation of a peroxy radical **Y** through combination with molecular oxygen (Atkinson and Arey, 2003). Panel B shows the oxidation of the hydroxynitrate acid product, $R^{20}COOH$, through hydrogen abstraction and reaction with molecular oxygen in R33 to peroxy radical **X**. Panel C shows in reaction R34 how a second nitrate radical can add to the newly generated double bond of the hydroxynitrate product of R7 (Fig. 8, main text). The nitrate radical adds to the less substituted C_7, leaving a relatively stable tertiary alkyl radical on C_2, which combines with O_2 via reaction R35 to form a peroxy radical **Z**.

Figure S8 shows how intermediates presented in Fig. 8 of the main text, **S**, **T**, and **U** combine with radicals **V**, **W**, **X**, **Y**, **Z** presented in Fig. S7 to produce the heavier MW products observed in aerosol filter extracts by UHPLC-MS via RO_2+RO_2 reactions. It is noted that each product in Fig. S8 may be formed from the combination of other intermediates not explicitly drawn in Fig. 8 in the main text and Fig. S7. These findings are in agreement with previous work showing the formation of organic peroxides during the oxidation of terpenes (Ng et al., 2008; Venkatachari and Hopke, 2008; Docherty et al., 2005). Figure S8 shows that the major heavy MW species in the UHPLC chromatogram of Fig. S5 can be generated from the same early oxidation intermediates **S**, **T**, and **U**, implying the possible existence of more than one isomer for each mass. The later observation is consistent with the EIC in Fig. S5 showing broad peaks in the UHPLC-MS for *m/z* 505, 522, and the later 489, and a clear shoulder for *m/z* 473.

Model Calculations for "RO_2+NO_3 dominant" Experiments

To ensure that the reaction conditions are favorable for the RO_2+NO_3 reaction, a simple chemical model is developed using the Master Chemical Mechanism (MCM v3.2) as a basis (Saunders et al., 2003). Reactions and their rate constants are shown in Table S1. The RO_2 fate in a typical "RO_2+NO_3 dominant" experiment (Experiment 5 in Table 1 of the main text) is shown in Fig. S10.

Reference

Atkinson, R., and Arey, J.: Gas-phase Tropospheric Chemistry of Biogenic Volatile Organic Compounds: A Review, Atmos. Environ., 37, 197-219, 2003.

Docherty, K. S., Wu, W., Lim, Y. B., and Ziemann, P. J.: Contributions of Organic Peroxides to Secondary Aerosol Formed from Reactions of Monoterpenes with O_3, Environ. Sci. Technol., 39, 4049-4059, 2005.

Neuman, J. A., Nowak, J. B., Huey, L. G., Burkholder, J. B., Dibb, J. E., Holloway, J. S., Liao, J., Peischl, J., Roberts, J. M., Ryerson, T. B., Scheuer, E., Stark, H., Stickel, R. E., Tanner, D. J., and Weinheimer, A.: Bromine measurements in ozone depleted air over the Arctic Ocean, Atmos. Chem. Phys., 10, 6503-6514, 10.5194/acp-10-6503-2010, 2010.

Ng, N. L., Kwan, A. J., Surratt, J. D., Chan, A. W. H., Chhabra, P. S., Sorooshian, A., Pye, H. O. T., Crounse, J. D., Wennberg, P. O., and Flagan, R. C.: Secondary Organic Aerosol (SOA) Formation from Reaction of Isoprene with Nitrate Radicals (NO_3), Atmos. Chem. Phys., 8, 4117-4140, 2008.

Odum, J. R., Hoffmann, T., Bowman, F., Collins, D., Flagan, R. C., and Seinfeld, J. H.: Gas/Particle Partitioning and Secondary Organic Aerosol Yields, Environ. Sci. Technol., 30, 2580-2585, 10.1021/es850943+, 1996.

Pavia, D., Lampman, G., Kriz, G., and Vyvyan, J.: Introduction to spectroscopy, Cengage Learning, 2008.

Sander, S. P., Abbatt, J., Barker, J. R., Burkholder, J. B., Friedl, R. R., Golden, D. M., Huie, R. E., Kolb, C. E., Kurylo, M. J., Moortgat, G. K., Orkin, V. L., andWine, P. H.: Chemical kinetics and photochemical data for use in atmospheric studies: Evaluation Number 17, Jet Propulsion Laboratory, 2011.

Saunders, S. M., Jenkin, M. E., Derwent, R. G., and Pilling, M. J.: Protocol for the development of the Master Chemical Mechanism, MCM v3 (Part A): tropospheric degradation of non-aromatic volatile organic compounds, Atmos. Chem. Phys., 3, 161-180, 2003.

Venkatachari, P., and Hopke, P. K.: Characterization of Products formed in the Reaction of Ozone with α-pinene: Case for Organic Peroxides, J. Environ. Monitor., 10, 966-974, 2008.

Vereecken, L., and Peeters, J.: A Theoretical Study of the OH-initiated Gas-phase Oxidation Mechanism of b-pinene ($C_{10}H_{16}$): First Generation Products, Phys. Chem. Chem. Phys., 14, 3802-3815, 10.1039/C2CP23711C, 2012.

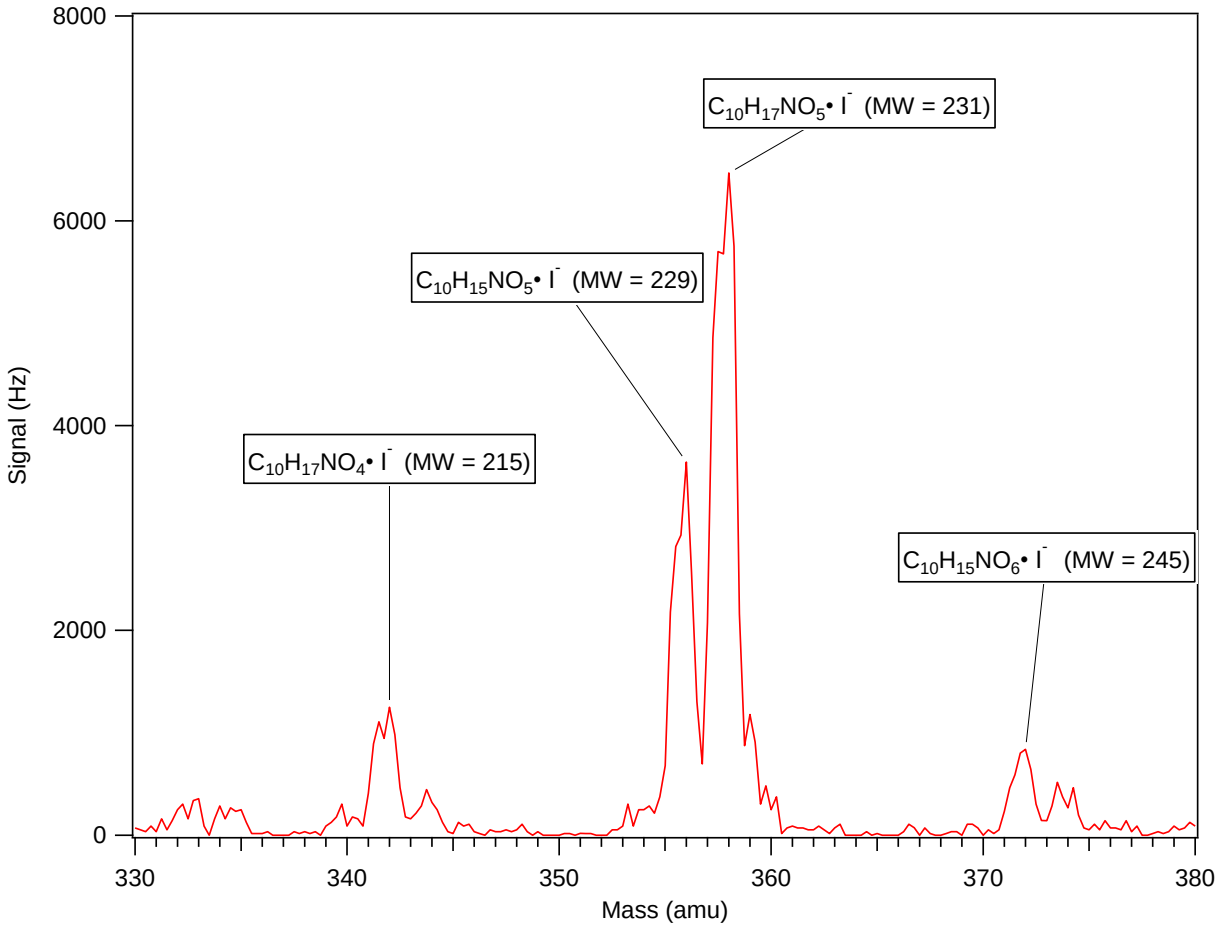

Figure S1: Chemical Ionization Mass Spectrometry (CIMS) spectra for a typical "RO_2+HO_2 dominant" experiment under dry conditions showing the major gas-phase compounds from the β-pinene+NO_3 reaction. The measured species are proposed to be organic nitrates due to their odd molecular weights. The specific molecular formulas for the ions shown are inferred from the chemical mechanism (Fig. 8, main text).

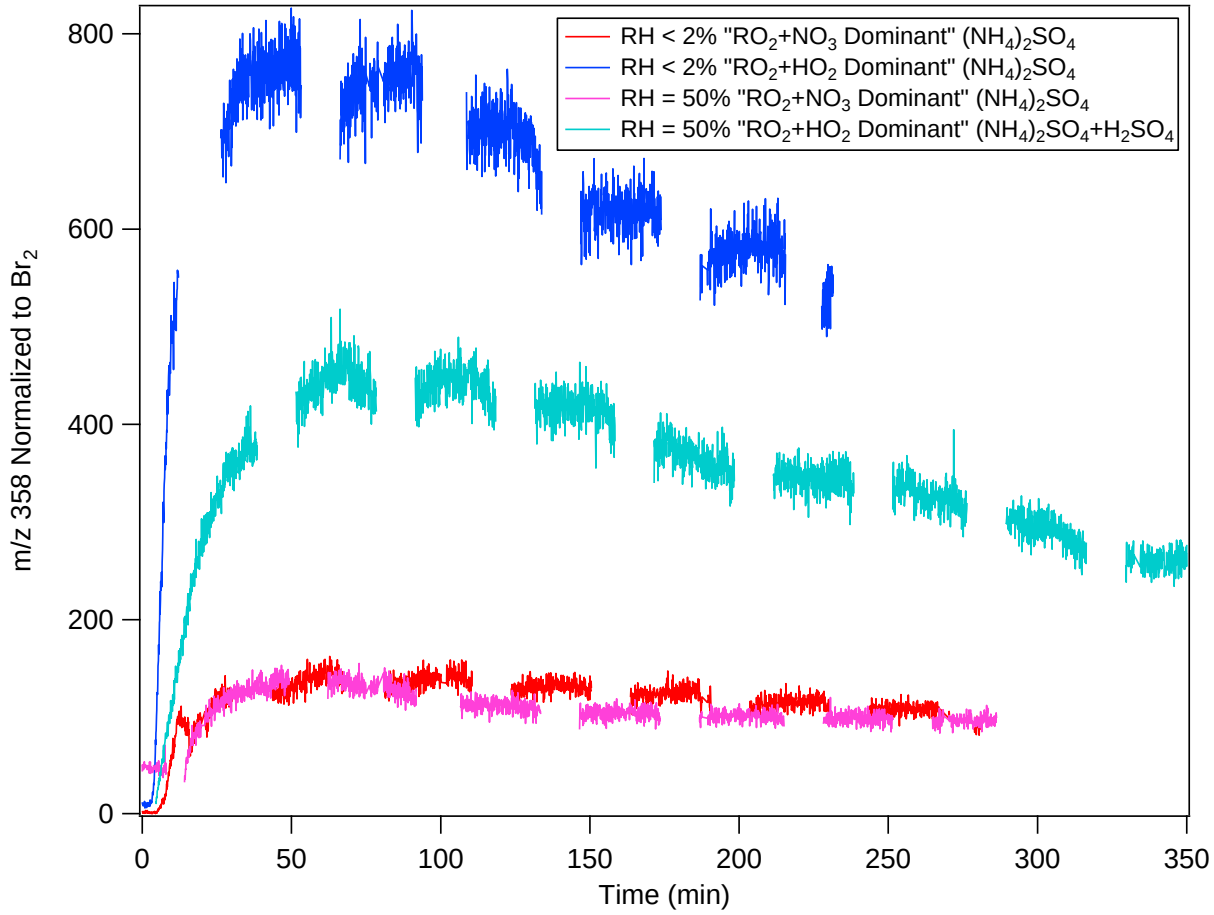

Figure S2: CIMS time series for *m/z* 358 for the β-pinene+NO_3 reaction at all conditions. *m/z* 358 corresponds to a molecule-iodide adduct where the molecule has a molecular weight of 231 amu. The signal is normalized to the instrument sensitivity to Br_2 to account for any sensitivity changes in the CIMS (Neuman et al., 2010). The species at *m/z* 358 is proposed to be either from a hydroperoxide (ROOH) or a dihydroxynitrate. It is significantly higher in experiments where RO_2+HO_2 is the dominant reaction pathway. Gaps in the data are from periodic measurements of the CIMS background. It is noted that the data shown above have not been corrected for CIMS background.

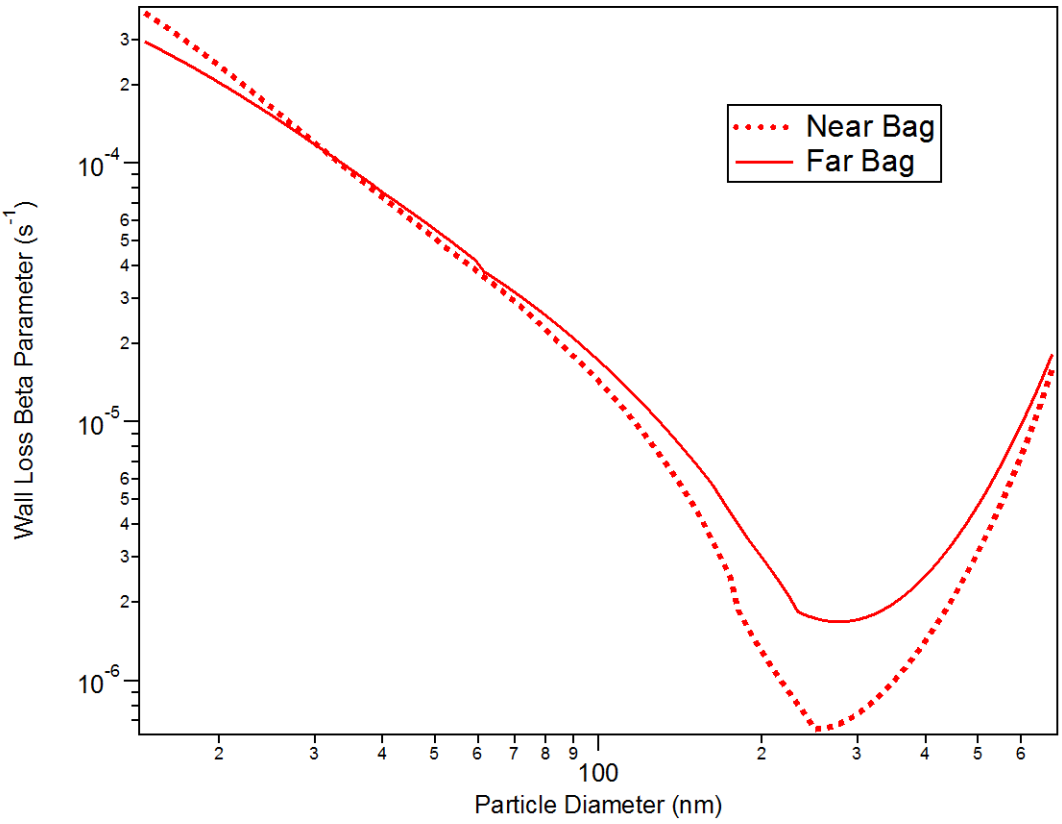

Figure S3: Size-dependent particle wall loss rates, β, calculated for both chambers at GTEC. Wall loss rates are determined by wall loss experiments performed using ammonium sulfate seed particles atomized from an 8 mM solution and measuring their decay over time. The first-order decay coefficients were measured for each particle bin over the course of each wall-loss experiment.

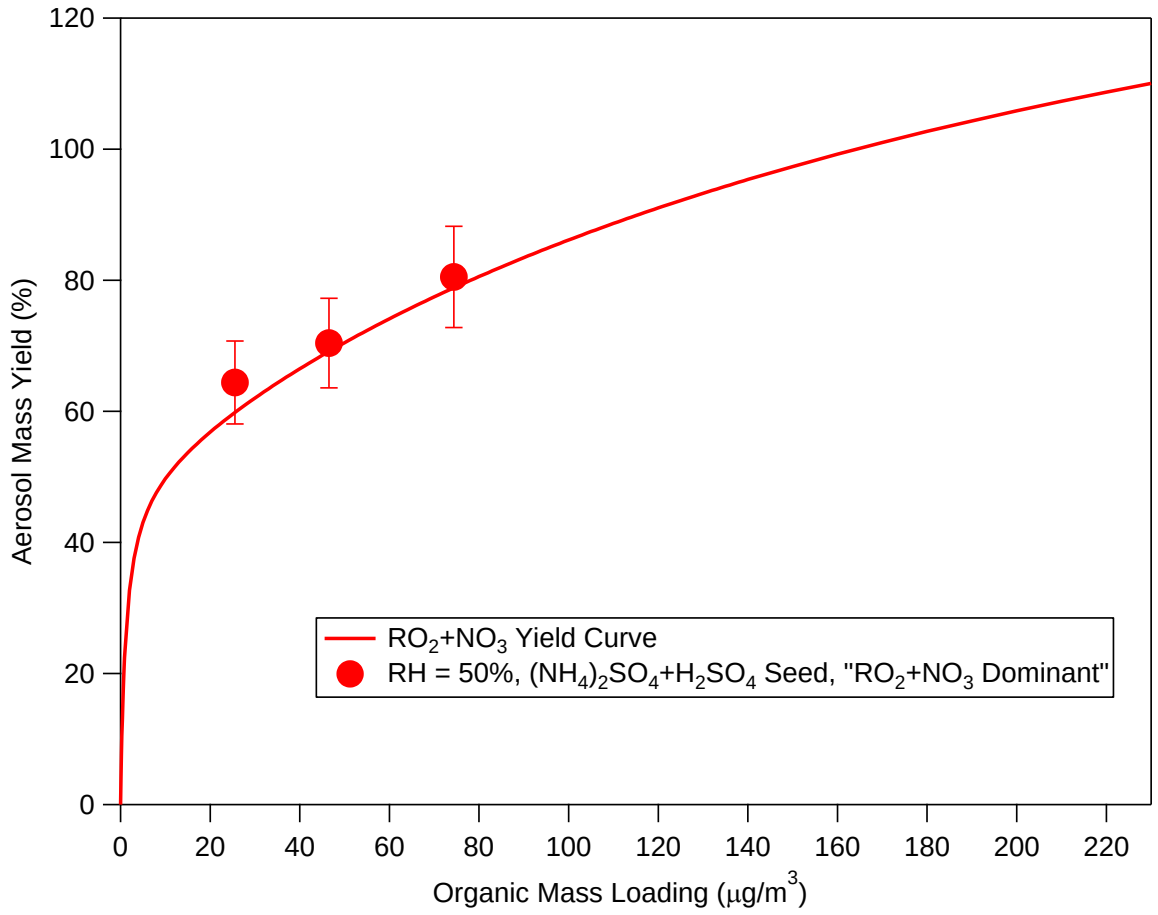

Figure S4: The yields for the experiments using $(NH_4)_2SO_4$+H_2SO_4 seed (circles) reported alongside the yields for the experiments using $(NH_4)_2SO_4$ seed (red curve) in "RO_2+NO_3 dominant" experiments. As seen in this figure, results from the experiments with $(NH_4)_2SO_4$+H_2SO_4 seed are in agreement with the yield curve generated by the two-product model (Odum et al., 1996) for experiments conducted in the presence of $(NH_4)_2SO_4$ seed.

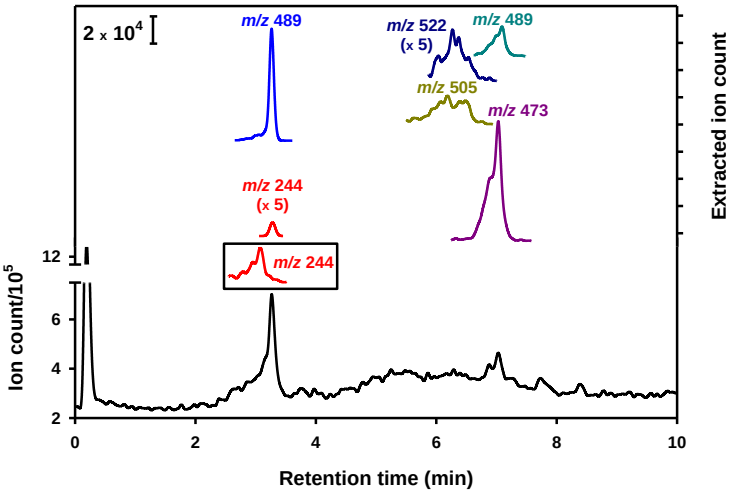

Figure S5: Total (bottom panel and left axis) and extracted (top panel and right axis) ion chromatogram (EIC) for eluting peaks at *m/z* 244, 489, 505, 522, and 473, and 489 in the UHPLC-MS chromatogram of a "RO_2+NO_3 dominant" experiment under dry conditions, in the presence of 0.1 mM HCOOH (fragmentor voltage = 50 v). The box shows the EIC for *m/z* 244 using 0.4 mM CH_3COOH instead of HCOOH (fragmentor voltage = 30 v).

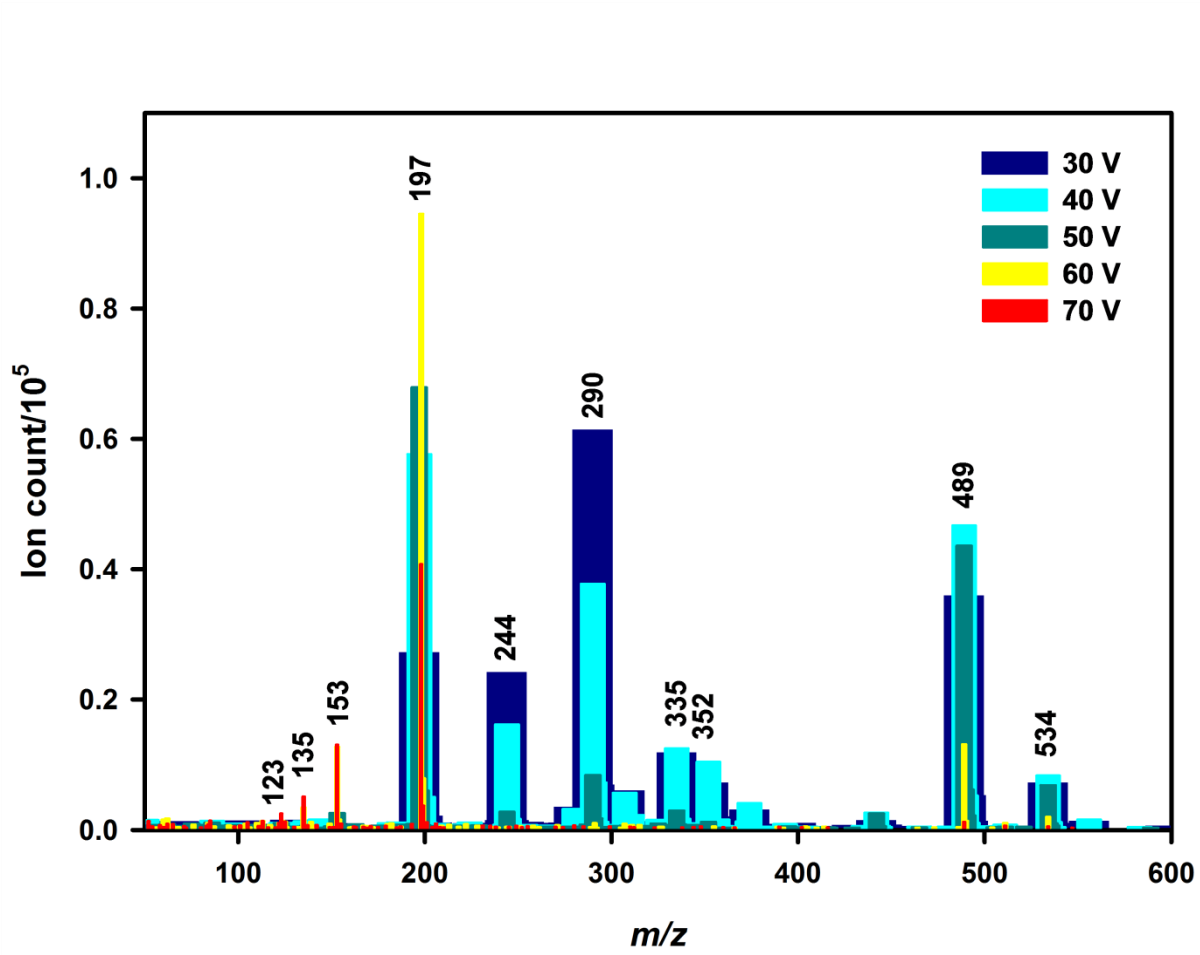

Figure S6: Collisional induced dissociation mass spectra of chromatographic peak in Fig. S5 at 3.27 ± 0.03 min between 30 and 70 V.

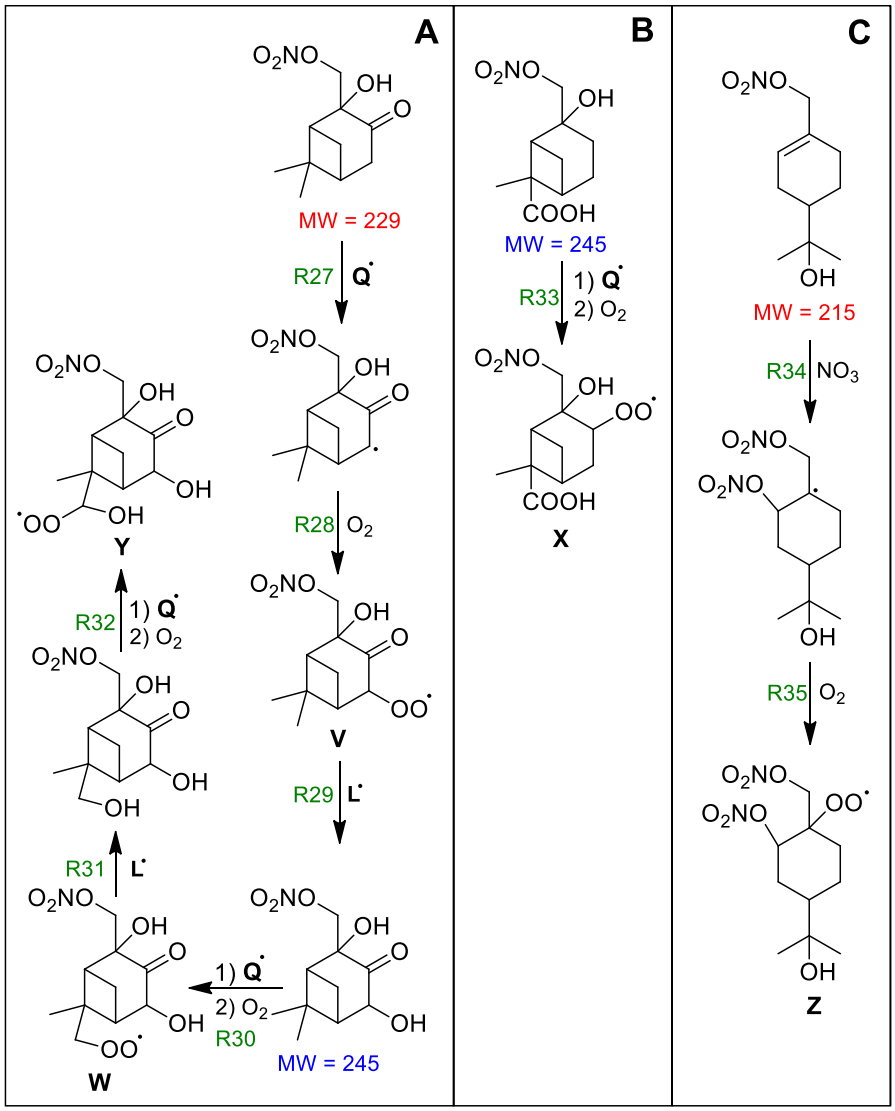

Figure S7: Proposed pathways for the further oxidation of products proposed in Fig. 8 of the main text. Named radicals are proposed to react to form the higher molecular weight species in Fig. S8.

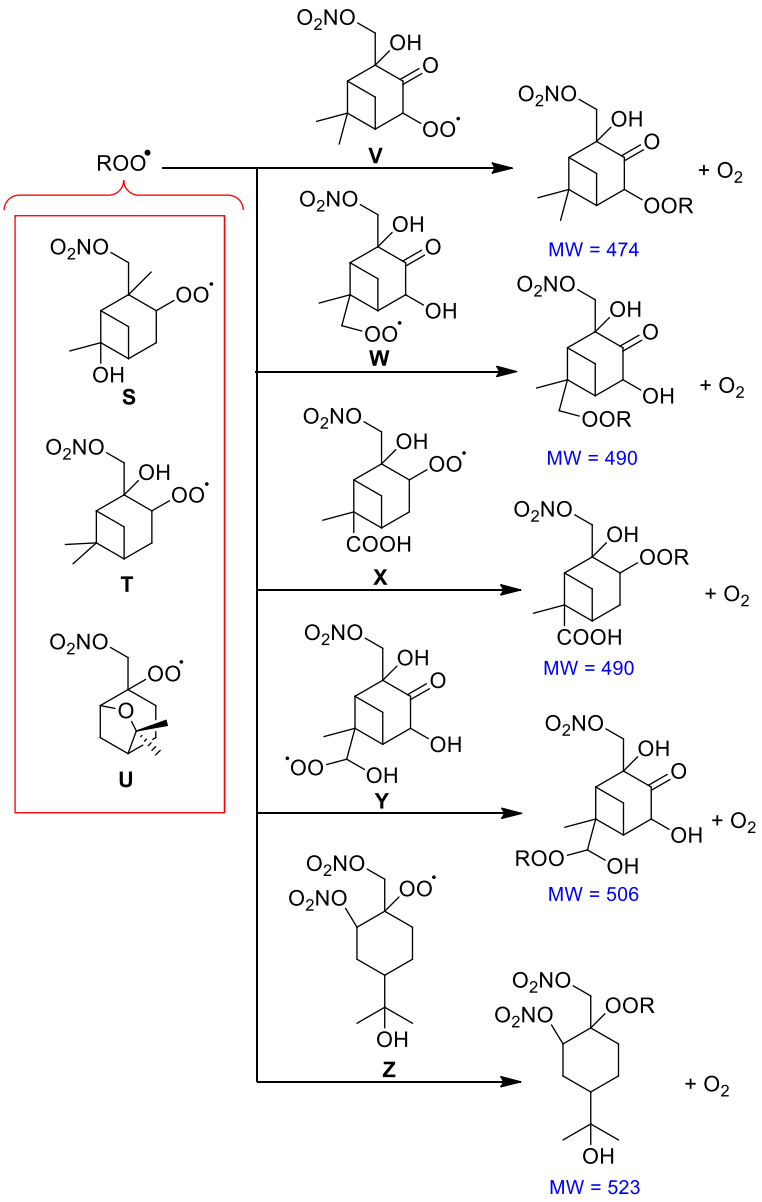

Figure S8: Proposed pathways for the production of organic peroxides from radicals **S**, **T**, and **U** (Fig. 8, main text) by reaction with radicals **V, W, X, Y, and Z** (Fig. S7, Supplement).

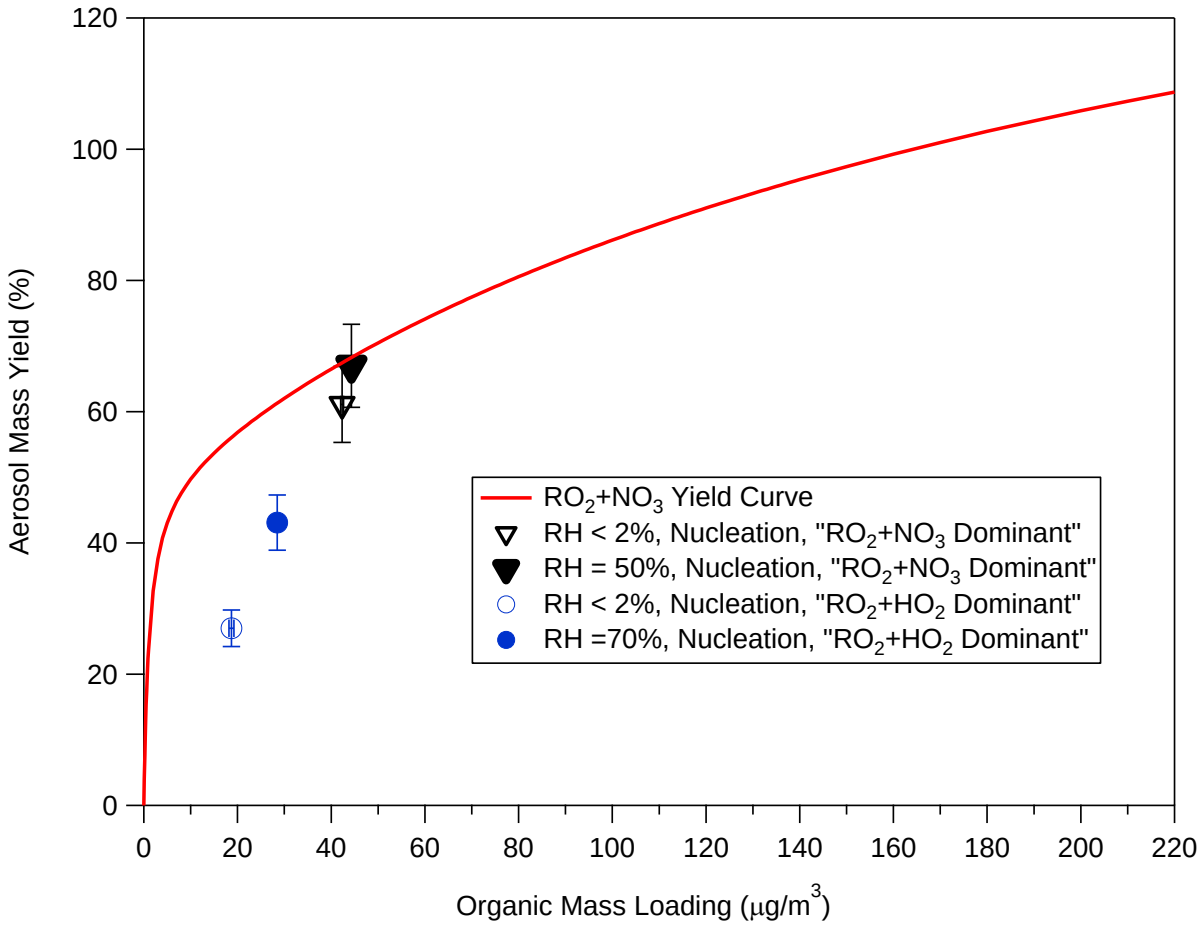

Figure S9: The yields for nucleation experiments for all conditions are reported alongside the yields for experiments with $(NH_4)_2SO_4$ seed. The yields from the nucleation and seeded experiments in the "RO_2+NO_3 dominant" experiments are in agreement with each other while the "RO_2+HO_2 dominant" experiments are significantly lower than under seeded conditions. The y-axis error bars represent uncertainty in yield calculated by an 8% uncertainty in chamber volume, 5% uncertainty in hydrocarbon injection, and one standard deviation of the aerosol volume measured by SMPS at peak growth.

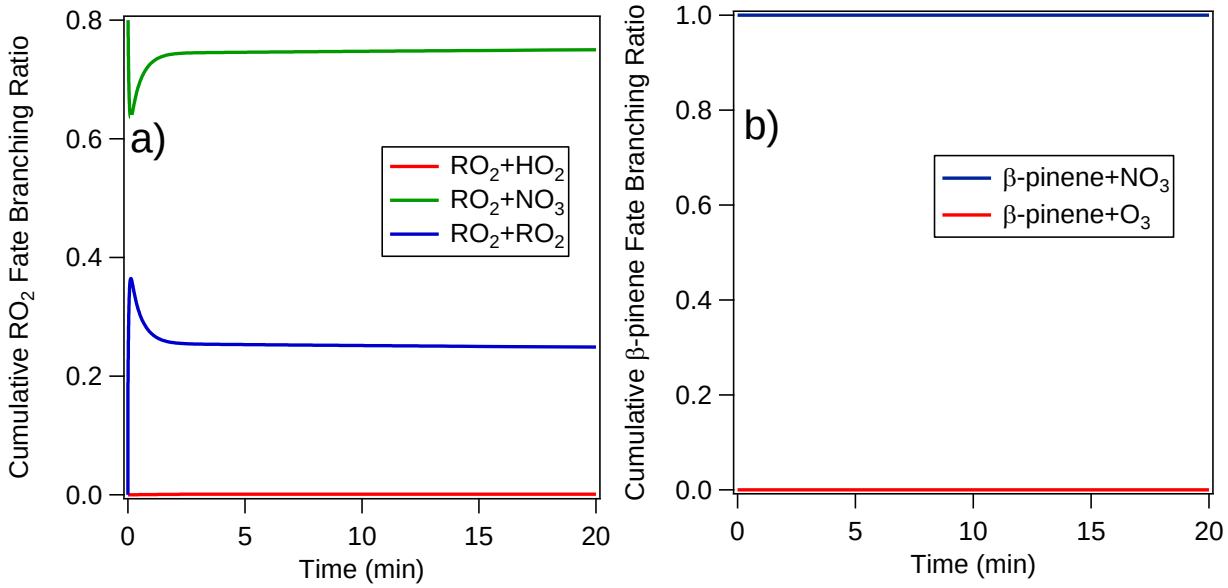

Figure S10: a) The RO_2 branching ratio and b) β-pinene fate for a typical "RO_2+NO_3 dominant" experiment (Experiment 5 in Table 1 of the main text). The branching ratios are determined from the reactions in the Master Chemical Mechanism (MCM v 3.2). The plots show the cumulative amount of products formed from each possible reaction.

Table S1: List of reactions and their rate constants for the β-pinene+NO_3 system. Reactions are adapted from MCMv3.2 (Saunders et al., 2003)[a].

Reaction:	**Rate Constant:**
$NO_2 + O_3 \rightarrow NO_3 + O_2$	$3.2 \cdot 10^{-17}$ cc molecules^{-1} s^{-1} [b]
$NO_2 + NO_3 \rightarrow N_2O_5$	$6.7 \cdot 10^{-12}$ cc molecules^{-1} s^{-1} [b]
$N_2O_5 \rightarrow NO_2 + NO_3$	$2.2 \cdot 10^{-1}$ s^{-1} [b]
$OH + O_3 \rightarrow HO_2 + O_2$	$7.3 \cdot 10^{-14}$ cc molecules^{-1} s^{-1} [b]
$OH + HO_2 \rightarrow H_2O_2 + O_2$	$1.1 \cdot 10^{-10}$ cc molecules^{-1} s^{-1} [b]
$HO_2 + O_3 \rightarrow OH + 2O_2$	$1.9 \cdot 10^{-15}$ cc molecules^{-1} s^{-1} [b]
$HO_2 + HO_2 \rightarrow H_2O_2 + O_2$	$1.4 \cdot 10^{-12}$ cc molecules^{-1} s^{-1} [b]
$NO + HO_2 \rightarrow NO_2 + OH$	$8.1 \cdot 10^{-12}$ cc molecules^{-1} s^{-1} [b]
$NO + O_3 \rightarrow O_2 + NO_2$	$1.9 \cdot 10^{-14}$ cc molecules^{-1} s^{-1} [b]
$NO + NO_3 \rightarrow 2\ NO_2$	$2.6 \cdot 10^{-11}$ cc molecules^{-1} s^{-1} [b]
$HCHO + NO_3 \rightarrow HNO3 + CO + HO_2$	$5.5 \cdot 10^{-16}$ cc molecules^{-1} s^{-1}
β-pinene + NO_3 + O_2 → NBPINAO2	$0.8 \cdot 2.51 \cdot 10^{-12}$ cc molecules^{-1} s^{-1}
β-pinene + NO_3 + O_2 → NBPINBO2	$0.2 \cdot 2.51 \cdot 10^{-12}$ cc molecules^{-1} s^{-1}
β-pinene + O_3 + O_2 → NOPINONE + CH200F	$0.4 \cdot 1.5 \cdot 10^{-17}$ cc molecules^{-1} s^{-1}
β-pinene + O_3 + O_2 → NOPINOOA + HCHO	$0.6 \cdot 1.5 \cdot 10^{-17}$ cc molecules^{-1} s^{-1}
NBPINAO2 + HO_2 → NBPINAOOH	$2.09 \cdot 10^{-11}$ cc molecules^{-1} s^{-1}
NBPINAO2 + NO → NBPINAO	$9.04 \cdot 10^{-12}$ cc molecules^{-1} s^{-1}
NBPINAO2 + NO_3 → NBPINAO	$2.3 \cdot 10^{-12}$ cc molecules^{-1} s^{-1}
NBPINAO2 + RO_2 → NBPINAO	$0.7 \cdot 9.2 \cdot 10^{-14}$ cc molecules^{-1} s^{-1}
NBPINAO → NOPINONE + HCHO + NO_2	10^{6} s^{-1}
NBPINAO2 + RO_2 → BPINBNO3	$0.3 \cdot 9.2 \cdot 10^{-14}$ cc molecules^{-1} s^{-1}
NBPINBO2 + HO_2 → NBPINBOOH	$2.09 \cdot 10^{-11}$ cc molecules^{-1} s^{-1}
NBPINBO2 + NO → NBPINBO	$9.04 \cdot 10^{-12}$ cc molecules^{-1} s^{-1}
NBPINBO2 + NO_3 → NBPINBO	$2.3 \cdot 10^{-12}$ cc molecules^{-1} s^{-1}
NBPINBO2 + RO_2 → NBPINBO	$0.6 \cdot 2 \cdot 10^{-12}$ cc molecules^{-1} s^{-1}
NBPINAO → NOPINONE + HCHO + NO_2	$7 \cdot 10^{3}$ s^{-1}
NBPINAO2 + RO_2 → BPINANO3	$0.2 \cdot 2 \cdot 10^{-12}$ cc molecules^{-1} s^{-1}

NBPINAO2 + RO_2 → NC91CHO	$0.6 \cdot 2 \cdot 10^{-12}$ cc molecules^{-1} s^{-1}
NC91CHO + NO_3 → NC91CO3	$2.32 \cdot 10^{-14}$ cc molecules^{-1} s^{-1}
NC91CO3 + HO_2 → NC91CO3H	$0.56 \cdot 1.39 \cdot 10^{-11}$ cc molecules^{-1} s^{-1}
NC91CO3 + HO_2 → NOPINONE + NO3 + OH + HCHO	$0.44 \cdot 1.39 \cdot 10^{-11}$ cc molecules^{-1} s^{-1}
NC91CO3 + NO → NOPINONE + HCHO + $2NO_2$	$1.98 \cdot 10^{-11}$ cc molecules^{-1} s^{-1}
NC91CO3 + NO_2 → NC91PAN	$9.4 \cdot 10^{-12}$ cc molecules^{-1} s^{-1}
NC91PAN →NC91CO3 + NO_2	$3.0 \cdot 10^{-4}$ s^{-1}
NC91CO3 + NO_3 → NOPINONE + HCHO + $2NO_2$	$4.0 \cdot 10^{-12}$ cc molecules^{-1} s^{-1}
NC91CO3 + RO_2 → NOPINONE+ HCHO + NO_2	10^{-11} cc molecules^{-1} s^{-1}
CH2OOFA → CH2OO	$0.37 \cdot 10^{6}$ s^{-1}
CH2OOFA → CO	$0.5 \cdot 10^{6}$ s^{-1}
CH2OOFA → HO_2 + CO + OH	$0.13 \cdot 10^{6}$ s^{-1}
CH2OO + CO → HCHO	$1.2 \cdot 10^{-15}$ cc molecules^{-1} s^{-1}
CH2OO + NO → HCHO	$1.0 \cdot 10^{-14}$ cc molecules^{-1} s^{-1}
CH2OO + NO_2→ HCHO	$1.0 \cdot 10^{-15}$ cc molecules^{-1} s^{-1}
CH2OO + H_2O→ HCHO	$6.0 \cdot 10^{-18}$ cc molecules^{-1} s^{-1}
CH2OO + H_2O→HCOOH	$1.0 \cdot 10^{-17}$ cc molecules^{-1} s^{-1}

[a]Unless otherwise noted, all reaction rates are from MCM v. 3.2

[b]Reaction rates are from Sander et al. (2011) and the references therein